

10 Gb/s operation of photonic crystal silicon optical modulators

Hong C. Nguyen,* Yuya Sakai, Mizuki Shinkawa, Norihiro Ishikura, Toshihiko Baba
Department of Electrical and Computer Engineering, Yokohama National University, 79-5 Tokiwadai, Hodogayaku,
Yokohama 240-8501, Japan
*hong@ynu.ac.jp

Abstract: We report the first experimental demonstration of 10 Gb/s modulation in a photonic crystal silicon optical modulator. The device consists of a 200 μm -long SiO_2 -clad photonic crystal waveguide, with an embedded p-n junction, incorporated into an asymmetric Mach-Zehnder interferometer. The device is integrated on a SOI chip and fabricated by CMOS-compatible processes. With the bias voltage set at 0 V, we measure a $V_{\pi}L = 0.028 \text{ V}\cdot\text{cm}$. Optical modulation is demonstrated by electrically driving the device with a $2^{31} - 1$ bit non-return-to-zero pseudo-random bit sequence signal. An open eye pattern is observed at bitrates of 10 Gb/s and 2 Gb/s, with and without pre-emphasis of the drive signal, respectively.

©2011 Optical Society of America

OCIS codes: (130.5296) Photonic crystal waveguides; (130.0250) Optoelectronics.

References and links

1. G. T. Reed, G. Mashanovich, F. Y. Gardes, and D. J. Thomson, "Silicon optical modulators," *Nat. Photonics* **4**(8), 518–526 (2010).
2. T. Tanabe, K. Nishiguchi, E. Kuramochi, and M. Notomi, "Low power and fast electro-optic silicon modulator with lateral p-i-n embedded photonic crystal nanocavity," *Opt. Express* **17**(25), 22505–22513 (2009).
3. X. N. Chen, Y. S. Chen, Y. Zhao, W. Jiang, and R. T. Chen, "Capacitor-embedded 0.54 pJ/bit silicon-slot photonic crystal waveguide modulator," *Opt. Lett.* **34**(5), 602–604 (2009).
4. X. L. Wang, C. Y. Lin, S. Chakravarty, J. D. Luo, A. K. Y. Jen, and R. T. Chen, "Effective in-device r_{33} of 735 pm/V on electro-optic polymer infiltrated silicon photonic crystal slot waveguides," *Opt. Lett.* **36**(6), 882–884 (2011).
5. G. Shambat, B. Ellis, M. A. Mayer, A. Majumdar, E. E. Haller, and J. Vučković, "Ultra-low power fiber-coupled gallium arsenide photonic crystal cavity electro-optic modulator," *Opt. Express* **19**(8), 7530–7536 (2011).
6. W. M. J. Green, M. J. Rooks, L. Sekaric, and Y. A. Vlasov, "Ultra-compact, low RF power, 10 Gb/s silicon Mach-Zehnder modulator," *Opt. Express* **15**(25), 17106–17113 (2007).
7. A. S. Liu, L. Liao, D. Rubin, H. Nguyen, B. Ciftcioglu, Y. Chetrit, N. Izhaky, and M. Paniccia, "High-speed optical modulation based on carrier depletion in a silicon waveguide," *Opt. Express* **15**(2), 660–668 (2007).
8. G. Rasigade, M. Ziebell, D. Marris-Morini, J. M. Fédéli, F. Milesi, P. Grosse, D. Bouville, E. Cassan, and L. Vivien, "High extinction ratio 10 Gbit/s silicon optical modulator," *Opt. Express* **19**(7), 5827–5832 (2011).
9. Q. F. Xu, S. Manipatruni, B. Schmidt, J. Shakya, and M. Lipson, "12.5 Gbit/s carrier-injection-based silicon micro-ring silicon modulators," *Opt. Express* **15**(2), 430–436 (2007).
10. T. P. White, L. O'Faolain, J. T. Li, L. C. Andreani, and T. F. Krauss, "Silica-embedded silicon photonic crystal waveguides," *Opt. Express* **16**(21), 17076–17081 (2008).
11. A. Berrier, M. Mulot, G. Malm, M. Östling, and S. Anand, "Carrier transport through a dry-etched InP-based two-dimensional photonic crystal," *J. Appl. Phys.* **101**(12), 123101 (2007).
12. D. Mori, S. Kubo, H. Sasaki, and T. Baba, "Experimental demonstration of wideband dispersion-compensated slow light by a chirped photonic crystal directional coupler," *Opt. Express* **15**(9), 5264–5270 (2007).
13. E. Ip, A. P. T. Lau, D. J. F. Barros, and J. M. Kahn, "Coherent detection in optical fiber systems," *Opt. Express* **16**(2), 753–791 (2008).
14. C. Y. Lin, X. L. Wang, S. Chakravarty, B. S. Lee, W. C. Lai, J. D. Luo, A. K. Y. Jen, and R. T. Chen, "Electro-optic polymer infiltrated silicon photonic crystal slot waveguide modulator with 23 dB slow light enhancement," *Appl. Phys. Lett.* **97**(9), 093304 (2010).

1. Introduction

Amongst the several types of silicon optical modulators [1], based on Mach-Zehnder interferometers (MZIs), μ -rings and electroabsorption, MZI modulators are considered

versatile as they are capable of both amplitude and phase modulation, as well as having a large working spectrum. Although advances in silicon MZI modulators have reduced their device size to millimeter-order, further reduction to sub-millimeter lengths is required for large-scale integration with other optical components. One way to achieve this is to incorporate slow-light structures, as their large group indices (n_g) result in a larger phase-shift for a given refractive index change. The increased phase-shifter efficiency can be exploited to reduce the device length, lower the operating voltage, or both. In terms of fabrication, it is also preferable to avoid rib-waveguide structures contained in most MZI modulators, as they require vertical partial-etching of the Si slab, which can be difficult to control and maintain uniformity across an entire wafer.

Photonic crystal waveguides (PCWs) are one such structures that satisfy both requirements – they exhibit slow-light while also not requiring the partial-etching mentioned above. PCWs can easily exhibit $n_g = 50$, which is over 10 times larger than in rib-waveguides often used in silicon MZI modulators, potentially reducing the device length by an order of magnitude. However, previously-reported PCW-based modulators have been demonstrated only at bitrates below 1.6 Gb/s, and furthermore, only using a simple, periodic 0-1 sequence signals [2–5].

In this paper, we report the first experimental demonstration of 10 Gb/s modulation in a PCW-MZI silicon optical modulator. Here we operate in the *semi-slow-light* regime of the PCW and *not* in the *slow-light* regime. Even then, $n_g > 10$ and so there is already some enhancement over rib-waveguide devices. The modulator incorporates a PCW phase-shifter of 200 μm length – the same as the shortest MZI modulator operating at 10 Gb/s that we are aware of [6] – and is fabricated through CMOS-compatible processes. While most modulators operate under either forward-bias [6], in which speed is limited by carrier diffusion, or reverse-bias which require long device lengths and/or large voltage swing [7,8], here we perform preliminary modulation experiments without a DC bias offset. Therefore modulation occurs predominantly by carrier-injection. To characterize the modulator performance, we electrically drive the device with non-return-to-zero (NRZ) pseudo-random bit sequence (PRBS) signals that are $2^{31} - 1$ bits in length. Furthermore, we pre-emphasize the drive signal to minimize the effect of carrier-diffusion which is slow [6,9]. Even in the *semi-slow-light* regime, we still observe clearly-open eye patterns at bitrates of 10 Gb/s and 2 Gb/s, using drive signals with and without pre-emphasis, respectively.

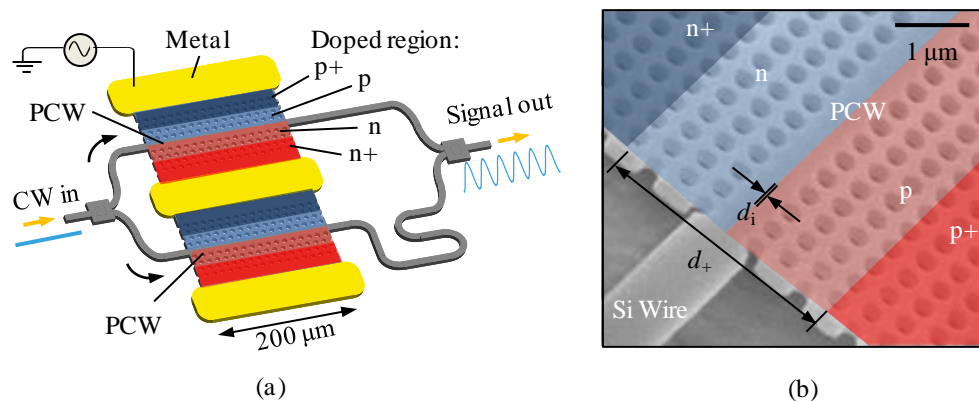


Fig. 1. (a) Schematic of PCW-MZI modulator. (b) SEM image of a typical PCW with SiO₂ cladding removed, overlaid with schematic of p/n doping regions, with $d_i = 0$ in this case.

2. Device description

Figure 1(a) shows a schematic of our device. A SiO₂-clad PCW [10] is embedded in each arm of the asymmetric MZI, which has a length asymmetry of 120.1 μm . The PCWs consist of a

W1 waveguide of length $L = 200 \mu\text{m}$ surrounded by a triangular lattice of holes, with a target diameter $2r = 215 \text{ nm}$ and pitch $a = 400 \text{ nm}$. The PCW is formed in a Si slab of 220 nm thickness, and is covered above and below by SiO_2 . Each PCW incorporates a p-n junction, consisting of moderately-doped p ($1 \times 10^{13} \text{ cm}^{-2}$) and n ($6 \times 10^{12} \text{ cm}^{-2}$) and highly-doped $p+$ and $n+$ (both $4 \times 10^{15} \text{ cm}^{-2}$) regions, placed symmetrically about the center of the PCW. The separations between the p and n , and $p+$ and $n+$ regions are defined as d_i and d_+ , respectively. Figure 1(b) shows a SEM image of a typical CMOS-fabricated PCW with the SiO_2 cladding removed. The figure also indicates schematically the doping region.

Figure 2(a) shows the I - V curves of the p-n junction embedded in the PCWs with a target $2r = 215 \text{ nm}$ and a range of d and d_+ . When $d_+ = 4 \mu\text{m}$ and d_i is varied from 0 to $3 \mu\text{m}$, the I - V curve changes only slightly, with the forward resistance R (slope of the curve) increasing by 11% from 29Ω to 32Ω . On the other hand, when $d_i = 0 \mu\text{m}$ and d_+ is increased from 4 to $8 \mu\text{m}$, the I - V curve becomes significantly shallower, and R increases by a factor of 2.7 from 29Ω to 79Ω . These results indicate that a smaller d_+ is preferred, although it must also be sufficiently large so as to not induce excessive optical loss.

Figure 2(b) compares the I - V curves for PCWs with target $2r = 215 - 245 \text{ nm}$ (normalized hole-diameter $2r/a = 0.54 - 0.61$), while $d_i = 0 \mu\text{m}$ and $d_+ = 4 \mu\text{m}$ are fixed. As $2r/a$ increases, the effective cross-section for carrier transport decreases, causing R to increase super-linearly from 29Ω to 120Ω as summarized in Table 1. While one may be tempted to reduce $2r$ to lower the resistance, we note that this will also affect strongly the optical properties of the PCW. Hence this is an optimization problem involving $2r$, a and the slab thickness, to maximize the electrical cross-section while simultaneously maintaining the desired PCW transmission bandwidth and slow-light properties.

We note that in Fig. 2(b) and Table 1, the increase in R by a factor of 4.2 is surprisingly large, given that $2r/a$ is increased merely by 14% . We believe that this is due to the depletion of carriers around the PCW holes, caused by surface damage and dopant-deactivation during the dry-etching process to form the PCW holes. This increases the electrical resistance across the PCW, increasing its effective filling-fraction [11]. To confirm this hypothesis, we perform a simplistic analysis as follows. We assume that the region around each PCW hole, defined by δ as shown in the inset of Fig. 2(b), is depleted of carriers and is highly resistive, such that the

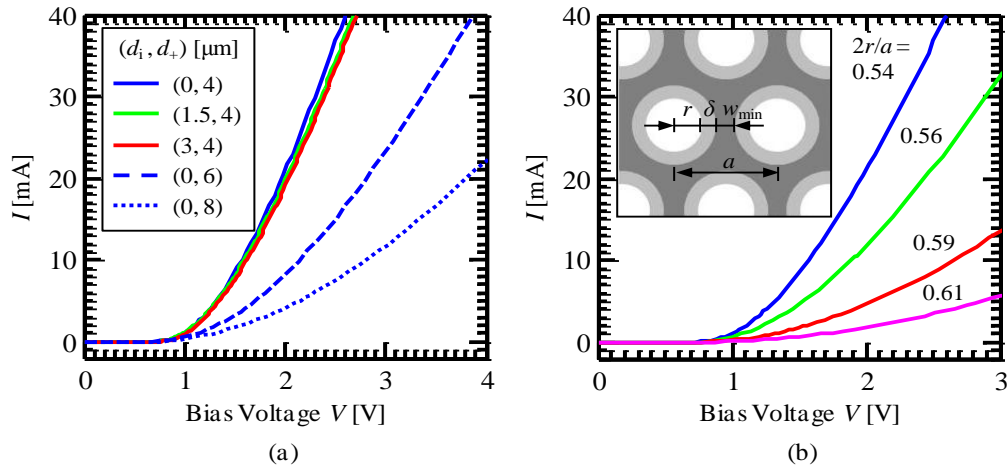


Fig. 2. I - V curves for (a) $2r/a = 0.54$ and varying d_i and d_+ ; (b) $d_+ = 4 \mu\text{m}$ and varying $2r/a$. Inset shows a schematic of PCW holes (white) surrounded by carrier-depleted (light-gray, defined by δ) and undamaged (dark gray) regions of the doped silicon.

Table 1. Measured And Estimated Values of Resistance And Normalized Hole-Diameter.

Target $2r$ [nm]	Target $2r/a$	R [Ω]	$R/R_{2r=215}$	$2(r + \delta)/a$ when $\delta = 73$ nm	$R_{\text{eff}}/(R_{\text{eff}} _{2r=215})$ when $\delta = 73$ nm
215	0.54	29	1	0.90	1
225	0.56	43	1.5	0.93	1.3
235	0.59	77	2.7	0.95	2.1
245	0.61	120	4.2	0.98	4.3

effective normalized-hole-diameter is $2(r + \delta)/a$. Since the effective resistance R_{eff} is strongly influenced by the effective inter-hole distance $w_{\text{min}} = a - 2(r + \delta)$, we make a simple approximation that $R_{\text{eff}} \propto 1/w_{\text{min}}$, which diverges to infinity as $2(r + \delta)/a \rightarrow 1$. We then compare the relative resistance, $R_{\text{eff}}/(R_{\text{eff}}|_{2r=215})$, for a range of δ . As summarized in Table 1, when $\delta = 73$ nm, the estimated relative resistance ($R_{\text{eff}}/[R_{\text{eff}}|_{2r=215}] = 1.3, 2.1, 4.3$) is very similar to the experimentally measured values ($R/R_{2r=215} = 1.5, 2.7, 4.2$), for $2r = 225, 235$ and 245 nm. Despite our simplistic approximation, this analysis supports the hypothesis of dry-etching-induced carrier-depletion. It suggests that the effective normalized-hole-diameter in our device is ≥ 0.90 , causing the large increase in R observed in Fig. 2(b) and Table 1. While there may be other factors behind the large increase in R , we believe the carrier-depletion is a major contributor. Therefore, such phenomenon also needs to be considered in the design and fabrication of carrier-based PCW devices.

The optical insertion loss of the device, integrated on-chip with low-loss spot-size converters, is as low as 13 dB fiber-to-fiber and is better than the previously-reported PCW-MZI modulators [3, 4]. This includes 6 dB coupling loss through the spot-size converters, which can be reduced further by improving the lithographic processes to sharpen the Si waveguide taper. The 7 dB on-chip loss includes ~ 2 dB from the MZI and the remainder from coupling into and out of the PCW, both of which can be reduced by improved fabrication. Furthermore, for the devices with $d_i = 0 - 3 \mu\text{m}$ and $d_+ = 4 - 8 \mu\text{m}$, we observe no definitive increase in optical loss. Therefore when $d_+ = 4 \mu\text{m}$, the $p+$ and $n+$ regions are sufficiently separated from the center of the PCW to not cause additional optical losses, at least in the fast-light regime. Thus experiments reported hereafter are performed on a PCW-MZI device in which $d_i = 0 \mu\text{m}$ and $d_+ = 4 \mu\text{m}$, which has $R = 29 \Omega$ and an estimated capacitance (limited by measurement apparatus) of < 800 fF, and hence a high-frequency RC cutoff of > 7 GHz.

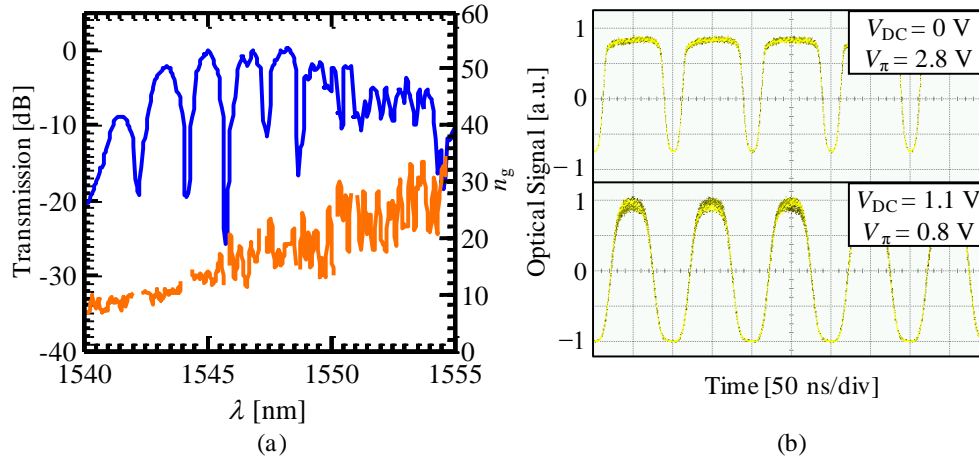


Fig. 3. (a) Transmission and n_g spectra of the PCW-MZI device. (b) Oscilloscope traces of the optical signal modulated by a 10 MHz sinusoidal electrical signal, with a peak-to-peak drive voltage corresponding to V_{π} , at different V_{DC} .

Figure 3(a) shows the transmission spectrum of the PCW-MZI device, normalized to the peak transmission. Oscillations occur in the spectrum due to the asymmetric nature of the MZI. Figure 3(a) also shows the n_g spectrum, obtained from group delay measurements using the modulation phase shift method [12]. This method gives inaccurate results around the transmission dips in Fig. 3(a) where the MZI arms interfere destructively, hence n_g at these wavelengths are not shown. As λ increases towards the band-edge, n_g increases. However, both the transmission and n_g spectra become noisy at long λ . This is because a slight shift in the PCW bandwidth between the MZI arms, due to fabrication imperfections, will result in a large and random phase-shift particularly in the slow-light regime, and manifest as noise in the spectra. We perform our modulation experiments in the *semi-slow*-light regime near $\lambda = 1547$ nm, where the free-spectral range FSR ≈ 1.7 nm and extinction ratio ER > 11.5 dB. Even in the fast-light regime, generally $n_g \approx 5 - 10$ such that the PCW already has a n_g -enhancement compared to rib-waveguides. Here we estimate $n_g \approx 18$ around the operating wavelengths, potentially giving rise to ~ 4 times n_g -enhancement. Note that the enhancement of the overall device efficiency is not so straight-forward to estimate, since the electrical and carrier transport characteristics also play a role.

We measure the electrooptic efficiency of the device, V_π , under AC conditions so that it is not obscured by slow thermo-optic effects. We modulate the optical signal with a 10 MHz sinusoidal electrical signal, and increase the drive amplitude until the optical peaks/troughs begin to overturn. Figure 3(b) show the oscilloscope traces of the modulated optical signal at different bias voltages. Without a DC bias, we measure $V_\pi = 2.8$ V. It is a relatively large value, however we note that the drive signal voltage varies from -1.4 V to $+1.4$ V, but the negative voltage part results in little phase-shift. In this case the peaks of the optical signal correspond to a negative drive voltage, hence becoming flat-topped – the optical signal is vertically asymmetric about zero. On the other hand, when the device is forward-biased to $V_{DC} = 1.1$ V, we measure $V_\pi = 0.8$ V and the optical signal becomes more sinusoidal and vertically symmetric, because the drive voltage is now operating completely in the carrier-injection regime, from $+0.7$ V to $+1.5$ V. These values of V_π correspond to a figure of merit $V_\pi L = 0.056$ V·cm and 0.016 V·cm, which are comparable to or smaller than other carrier-injection type MZI modulators [6].

3. Modulation experiments

3.1 Multi-Gb/s modulation

Optical modulation is performed in single-ended mode by driving the p-n junction in one of the PCW-MZI arms. The electrical driving signal, produced by a combination of an electrical synthesizer and a pulse pattern generator (PPG), is amplified then combined with a DC bias through a bias-tee. This electrical signal drives the p-n junction, modulating the TE-polarized light from a tunable CW laser, coupled onto the chip via a lensed fiber. The output optical signal is amplified by an erbium-doped fiber amplifier, then passed through an O/E converter and detected on an Agilent 86100C/54754A sampling oscilloscope and 18 GHz detector set. Hereafter, all modulation experiments are performed at wavelengths in-between the transmission peak and dip of $\lambda = 1546.8$ nm and 1547.5 nm respectively.

Figure 4 shows the small-signal frequency response of the PCW-MZI, driven by a sinusoidal signal with a peak-to-peak voltage $V_{pp} = 0.25$ V and no bias ($V_{DC} = 0$ V). The normalized modulation depth of the optical signal decreases as the frequency is increased, with a 3 dB bandwidth of approximately 3 GHz.

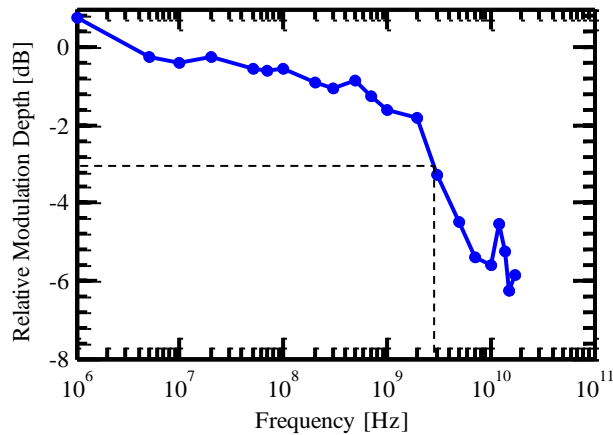


Fig. 4. Small-signal frequency response of the PCW-MZI modulator.

Figure 5 shows the eye patterns of the optical modulation signal at bitrates of 2 Gb/s (a), 5 Gb/s (b) and 10 Gb/s (c), without pre-emphasis. The device is driven by a $2^{31}-1$ bit NRZ PRBS signal generated by an Anritsu MP181020A PPG. Zero bias is applied to the drive signal ($V_{DC} = 0$ V) and $V_{pp} = 2.0 - 2.6$ V as indicated on each eye diagram. V_{pp} is adjusted so that the eye visually appears most “open” at each data rate – it is reduced at higher bitrates since large V_{pp} results in increased carrier injection and timing jitter, degrading the eye quality further. The inset of the 10 Gb/s eye diagram shows the input drive signal. We see that the eye is clearly open at 2 Gb/s, with ER = 7.2 dB and eye signal-to-noise ratio (SNR) of 4.3 dB, while the transmission increases by 1.0 dB due to carrier extraction. In comparison, earlier work on PCW modulators have only demonstrated simple, periodic 0-1 sequence modulation, and furthermore, only at bitrates below 1.6 Gb/s [2–5]. Hence this is the first time that optical modulation at bitrates above 2 Gb/s has been reported in PCW-based modulators, and furthermore, performed using PRBS signals.

While the eye is open at 2 Gb/s, it is hardly open at 5 Gb/s and completely closed at 10 Gb/s. Upon close inspection of the eye patterns, we find that the fall-time τ_{fall} of the 2 Gb/s eye pattern is comparatively slow at ~ 450 ps and has small jitter, while the rise-time τ_{rise} is faster at ~ 150 ps but with large jitter of 260 ps peak-to-peak. In our experiment, the 0-level corresponds to the carrier-injected state, hence the slow τ_{rise} is due to the slow injection of carriers by diffusion. On the other hand, the negative voltage of the drive signal helps extract the carriers to result in the faster τ_{fall} , although this depends on the concentration of injected carriers for various bit sequences and hence has large jitter. We can see from Fig. 5 that the closing of the eye pattern at high bitrates is predominantly due to the τ_{rise} jitter – a result of the inefficient extraction of carriers. In order to open the eye at higher bitrates, we overcome this limitation by pre-emphasizing the driving signal, as described below.

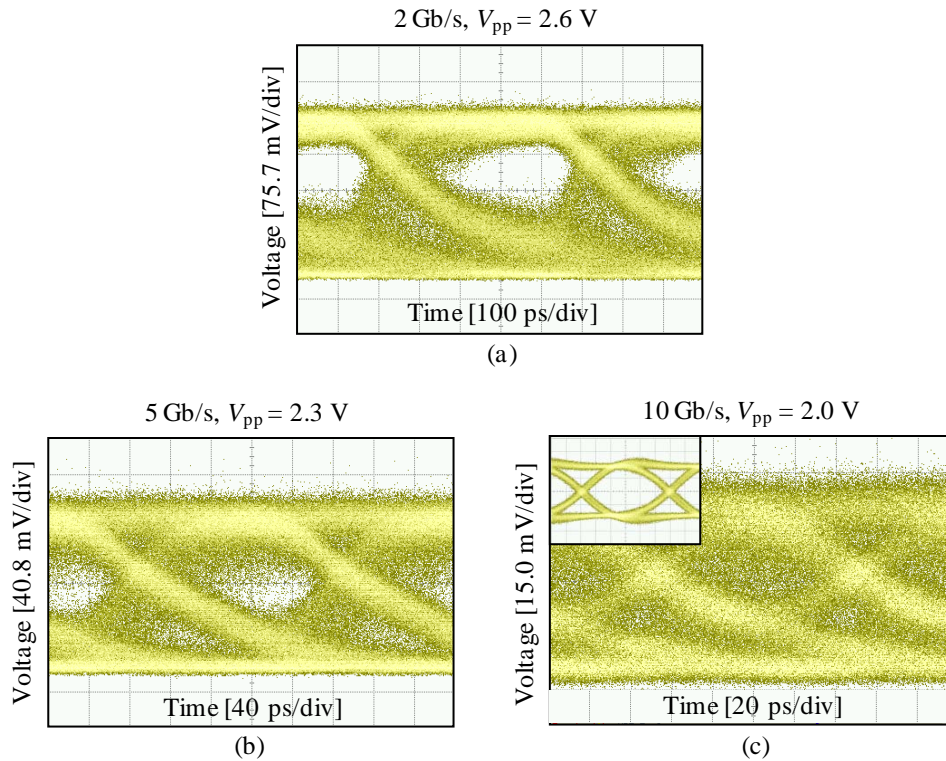


Fig. 5. Eye diagrams of the optical modulation signal without pre-emphasis, at (a) 2 Gb/s, (b) 5 Gb/s and (c) 10 Gb/s. Inset in (c) shows the eye diagram of the 10 Gb/s drive signal.

3.2 Pre-emphasis for modulation at 10 Gb/s

Figure 6 shows the modulation results at 10 Gb/s using pre-emphasized drive signals [6,9]. (a) shows the eye pattern of the pre-emphasized drive signal produced from the built-in PPG of Alnair Labs SeBERT-1040C bit error rate tester. The signal has $V_{DC} = 0$ V and an amplitude of 1.8 V, and $V_{pp} = 4.2$ V including the pre-emphasis spike. We note that the eye is measured with an 18 GHz detector, and the actual overshoot of the pre-emphasis may be sharper and stronger than observed in Fig. 6(a). Figure 6(b) shows the eye pattern of the modulated optical signal, with the eye clearly-open. For this signal, the additional in-device optical loss is 2.8 dB (total on-chip loss of 9.8 dB) while the eye ER = 7.9 dB and SNR = 4.6 dB. At a received power of -4.6 dBm the bit-error rate is measured to be 1.3×10^{-4} , which is below the typical threshold (10^{-3}) for receivers employing forward error-correction [13]. In this case the electrical power of the drive signal is measured to be 29 mW, corresponding to an energy of 2.9 pJ/bit. This is nearly 2 orders larger than ring-type modulators, but still is the smallest for a MZI modulator as far as we are aware [1, 6]. Nevertheless the modulation characteristics can be further improved by optimizing the operating condition such as the fast/slow-light regime and pre-emphasis. Optimization of the device structure such as the PCW parameters and the doping profile will also be beneficial. While there are rooms for improvement of the device, we emphasize that this is the first experimental demonstration of 10 Gb/s modulation in a PCW optical modulator.

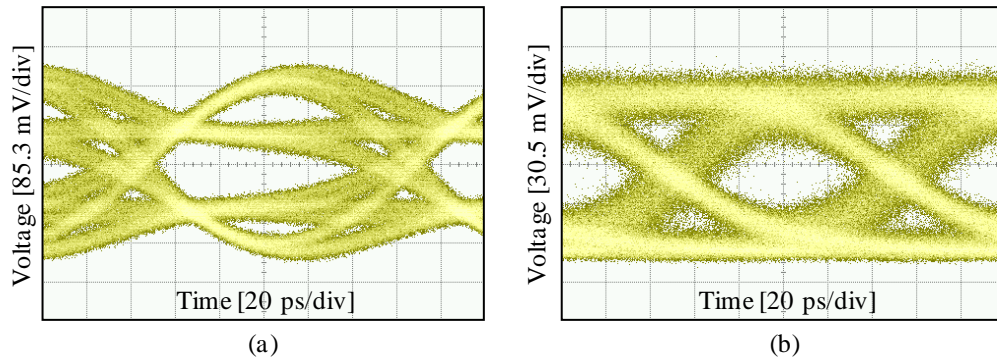


Fig. 6. Eye diagrams for 10 Gb/s modulation with pre-emphasis: (a) drive signal after 20 dB attenuation; (b) modulated optical signal.

4. Conclusion

In summary we have reported the first experimental demonstration of 10 Gb/s modulation in a photonic-crystal silicon optical modulator. The device incorporates PCW phase-shifters of 200 μm length, which is the same as the shortest MZI modulator capable of 10 Gb/s modulation that we are aware of [6]. The PCW-MZI modulator was operated in the *semi-slow-light* regime, and driven by $2^{31}-1$ bit NRZ PRBS signals with no bias ($V_{\text{DC}} = 0$ V). An open eye was observed at 2 Gb/s bitrate with $V_{\text{pp}} = 2.6$ V and no pre-emphasis. An open eye was also observed at 10 Gb/s by pre-emphasizing the driving signal to 1.8 V amplitude and 4.2 V peak-to-peak including the pre-emphasis, corresponding to an energy consumption of 2.9 pJ/bit. These results exceed earlier work on PCW modulators, which reported modulation using only periodic 0-1 sequence signals, and furthermore, only at bitrates below 1.6 Gb/s [2,3,5,14]. We anticipate further improvements in the modulator performance by optimizing the PCW and doping parameters, as well as by optimizing the modulation condition such as the signal pre-emphasis. Furthermore, operating in the large- n_g *slow-light* regime can lead to further improvements in the modulation characteristics as well as reduction of the device length and/or the drive voltage [14]. However, we note that even in the *fast-light* regime, PCW modulators generally have a slow-light enhancement factor of 2 or more compared to rib-waveguide devices. In addition, there is also the merit of not requiring the vertical partial-etching of the Si slab during device fabrication.

Acknowledgements

This work was partly supported by the FIRST Program of JSPS.